Release of a reliable open-source package for performance evaluation of ocean renewable energy devices

Yingyi Liu[#1], Shigeo Yoshida[#2], Hiroshi Yamamoto[*3], Akinori Toyofuku[*4], Changhong Hu[#5], Makoto Sueyoshi[#6], Hongzhong Zhu[+7]

[#]*Research Institute for Applied Mechanics, Kyushu University, Kasuga 816-8580, JAPAN*

[*]*Interdisciplinary Graduate School of Engineering Sciences, Kyushu University, Kasuga 816-8580, JAPAN*

[+]*Research and Education Center for Advanced Energy Materials, Devices and Systems, Kyushu University, Kasuga 816-8580, JAPAN*

[1]liuyingyi@riam.kyushu-u.ac.jp

[2]yoshidas@riam.kyushu-u.ac.jp

[3]yamamotoh@riam.kyushu-u.ac.jp

[4]toyofukua@riam.kyushu-u.ac.jp

[5]hu@riam.kyushu-u.ac.jp

[6]sueyoshi@riam.kyushu-u.ac.jp

[7]zhuhongzhong@riam.kyushu-u.ac.jp

Abstract— **Marine renewable energy (MRE) devices, such as offshore wind turbines, wave energy converters and tidal energy converters, are usually in the form of floating types and anchored by mooring systems. To analyze the feasibility of these floating systems in an efficient manner with respect to a wide band of frequency, frequency domain methods are good options to choose. In the present work, we developed an efficient software package for evaluating the performance of floating renewable energy systems in the coastal and offshore regions. It aims to contribute an open-source effort to numerical simulations for ocean energy converters. The interface and structure of the software package are introduced in detail so as to let it be well understandable by the readers. Computations of a benchmark geometry and two practical applications of floating wind turbine are conducted and compared with theoretical results, experimental data and results from commercial software Hydrostar, justifying the effectiveness of the developed software package.**

Keywords— **offshore wind energy; wave energy; floating structure; performance evaluation; potential flow theory**

I. INTRODUCTION

Due to the explosion of energy consumption in household life, industrial production and public service over the last several decades [1], the fossil resources are getting exhausted. In recent years, the coastal/ offshore renewable energies, such as offshore wind energy [2], wave energy [3], and tidal energy [4], etc., are becoming promising alternatives for the traditional fossil energies.

Hydrodynamic loads have significant influences on the substructures of these offshore energy devices [5]. Wang et al. [6] and Liu et al. [7] reviewed the recent advancements of floating foundations for particularly the offshore wind turbines (OWTs) which have been turned into industrial applications, and Oh et al. [8] further discussed their future trends and challenges. Note that in the design process of the ocean energy devices, one of the critical considerations is to evaluate their feasibility under some localized sea conditions (see e.g. [9] and [10]), i.e., to compute their wave loads and motion responses [11] under various circumstances. These devices frequently employ floating foundations in the form of spar, tension-leg spar, semi-submersible, raft, and buoyancy-stabilized floater, etc., which are designed to be installed under the water depth going from approximately 20 meters to around 200 meters. Within such a range of moderate water depth, for the consideration of the offshore structure safety, it is more reasonable to use the finite-depth wave theory instead of assuming the installation water depth to be infinity.

II. THEORY AND ALGORITHM

Evaluation of the free-surface Green's function G(**x**; **ξ**) is one of the most essential tasks in the analysis of wave-structure interactions within the potential flow framework. In order to elucidate the target problem with a deep understanding of the physics, the basic mathematical theory and the developed numerical algorithm for evaluation of the free-surface Green's function are clearly presented below.

A. Governing equation and boundary conditions

The Green's function G(**x**; **ξ**), or source potential, is usually defined as the velocity potential at the point (ξ, η, ζ) due to a point source of strength -4π located at the field point (x, y, z). Mathematically, the free-surface Green's function satisfies the following equation in the fluid domain,

$$\left(\frac{\partial^2}{\partial x^2}+\frac{\partial^2}{\partial y^2}+\frac{\partial^2}{\partial z^2}\right)G(x,y,z;\,\xi,\eta,\zeta)$$

$$= \delta(x-\xi)(y-\eta)(z-\zeta) \quad (1)$$

and corresponding boundary conditions can be expressed as

$$\left.\begin{array}{ll} \frac{\partial G}{\partial z} = vG & z = 0 \\ \frac{\partial G}{\partial z} = 0 & z = -h \\ \lim_{R\to\infty}\left[\sqrt{vR}\left(\frac{\partial G}{\partial R} - \mathrm{i}vG\right)\right] = 0 & R \to \infty \end{array}\right\}, \quad (2)$$

where δ is the Dirac delta function, $v = \omega^2/g$ is the wave number in deep water, and R is the horizontal distance between the source point and the field point.

B. A new algorithm based on region-decomposition strategy

The entire parametric domain of interest is decomposed into four sub-regions with respect to R/h and appropriate series or asymptotic expansions are applied in different sub-regions. Based on this strategy, the non-trivial integration form of the Green's function, can be avoided throughout the entire domain. In addition to that, fast convergence at the neighborhood of $R = 0$ can be achieved. Details of the present algorithm are given below.

In the first outside region when $R/h > 0.5$, the eigenfunction expansion is employed as suggested by Newman [12]:

$$G = \mathrm{i}\frac{\pi}{N_0}\cosh k(z+h)\cosh k(\zeta+h)H_0^{(1)}(kR) + \sum_{m=1}^{\infty}\frac{2}{N_m}\cos\mu_m(z+h)\cos\mu_m(\zeta+h)K_0(\mu_m R), \quad (3)$$

where $H_0^{(1)}$ denotes Hankel function of the first kind, and K_0 denotes modified Bessel function of the second kind. The denominators N_m $(m = 0,1,\ldots)$ are functions of the imaginary roots of the dispersion equation.

In the intermediate region when $0.05 \leq R/h < 0.5$, a nonlinear series-acceleration method named "Epsilon Algorithm" (Wynn [13] and Mishonov & Penev [14]) has been implemented in FinGreen3D. The Epsilon Algorithm is successfully incorporated with the eigenfunction expansion.

In the second intermediate region when $0.0005 \leqslant R/h < 0.05$, convergent results of eigenfunction expansion in Eq. (3) can no longer be achieved using the Epsilon-Algorithm-accelerated method. This urges us to search for another possible way of accelerating the convergence of the series. In this region, the following formulation is derived based on Pidcock [15], with an improvement on the calculation of the Rankine-source summation:

$$G = \frac{1}{r} + \frac{1}{r_1} + \sum_{p=1}^{\infty}(Rs)_p + \frac{2}{h}\left[\gamma + \log\left(\frac{R}{4h}\right)\right] + \mathrm{i}\Lambda H_0^{(1)}(kR) + 4\sum_{m=1}^{\infty}\left[C_m^{(1)}K_0(\mu_m R) - C_m^{(2)}K_0(\mu_m^* R)\right], \quad (4)$$

where γ denotes the Euler constant, μ_m^* is an approximation of μ_m when m is large, i.e., $\mu_m^* = m\pi/h$. $C_m^{(1)}$, $C_m^{(2)}$ and Λ are series expansion coefficients. The principle of Eq. (4) is to accelerate the convergence through subtracting a simplified series with the same asymptotic form when m is large.

In the singular region when the parameter R/h approaches zero, all previous formulations become invalid due to their singularity in the neighbourhood of zero. A more suitable series expansion is therefore preferred, which should not contain any singularity near the origin (apart from the Rankine terms). The rapidly convergent representation of the free-surface Green's function proposed by Linton [16] using Ewald's method [17] is suitable for region D and hence is implemented

$$G = \mathrm{i}\frac{\pi}{N_0}\cosh k(z+h)\cosh k(\zeta+h)J_0(kR) + \sum_{m=1}^{\infty}\frac{\Lambda_m}{N_m}\cos\mu_m(z+h)\cos\mu_m(\zeta+h) + \frac{1}{r}\operatorname{erfc}\left(\frac{r}{ah}\right) + \frac{1}{r_1}\operatorname{erfc}\left(\frac{r_1}{ah}\right) + \sum_{i=1}^{4}\frac{1}{\left(R^2+\chi_i^2\right)^{1/2}}\operatorname{erfc}\left(\frac{\left(R^2+\chi_i^2\right)^{1/2}}{ah}\right) + 2v\int_0^{ah/2} e^{v^2t^2-R^2/4t^2}\sum_{i=1}^{4}e^{-v\chi_i}\operatorname{erfc}\left(\frac{\chi_i}{2t} - vt\right)\frac{\mathrm{d}t}{t}, \quad (5)$$

where erfc is the complementary error function, and χ_i are the vertical distance components.

III. Interface and Structure of the Software Package

The algorithm described in section II has been implemented in a released software package FinGreen3D which is written in Fortran 90. The input and output parameters to interact with hydrodynamic solvers in frequency domain are introduced in Table 3.

Table 1. Input and output variables of FinGreen3D

Variables	Data Type	Explanations
R	Input, REAL (8)	Horizontal distance between the field point and the source point
ZF, *ZP*	Input, REAL (8)	*z* coordinates of the field point and the source point, respectively
V	Input, REAL (8)	Corresponding wave number in deep water
WVN	Input, REAL (8)	Array, with *NK* elements, restoring the roots of the dispersion equation
NK	Input, INTEGER	Number of elements in the array *WVN*
H	Input, REAL (8)	Dimensional finite water depth
TAG	Input, INTEGER	A flag to determine whether the Rankine part is to be calculated or not
GRN	Output, Complex (16)	Array, values of Green's function and its derivatives with respect to *R* and *z*

The information of the field point and source point locations should be firstly given to the driver subroutine. $v = \omega^2/g$ is the deep water wave number, where ω is the wave angular frequency and g is the gravitational acceleration. *WVN* is a variable to store the roots of the water wave dispersion equation, in which the first element is the positive root k of the dispersion equation and the rest elements are the real roots, i.e., μ_m (m= 1,2…, *NK*-1). *NK* defines the size of the array *WVN*. *H* is the dimensional water depth and a positive real number should be given prior to the calculations. The integer variable *TAG* is used to determine whether the Rankine part is to be calculated (*TAG* =1) or not (*TAG* =0). The reason is that in some hydrodynamic solvers, especially in those applying the lower-order discretization, the Rankine part is normally integrated separately through an analytical algorithm [18]. Whereas for the other solvers applying the higher-order discretization, the Rankine part is normally integ-rated together with the wave-term in Green's function, taking advantage of some special strategies for the singular and near singular integrals [19]. *GRN* is a 3-element complex array defining the output of FinGreen3D, in which *GRN* (1) is the value of Green's function, *GRN* (2) and *GRN* (3) are the derivatives of Green's function with respect to *R* and *z*, respectively.

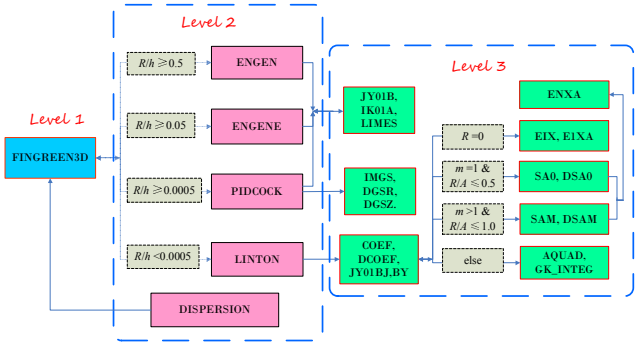

Fig. 1. Multi-level subroutines in the hierarchical code structure.

The driver subroutine, FINGREEN3D, is the only Level_1 subroutine, from which all the Level_2 subroutines are called. Level_2 subroutines are corresponding to the four expansion methods in the corresponding regions as described in Section 2, respectively. In addition to that, the Level_2 subroutines can also be implemented for other specific-purpose computations alone, as long as their necessarily associated subroutines are included. Level_3 subroutines consist of affiliated subroutines and external subroutines. The affiliated subroutines are called by two Level_2 subroutines, i.e., PIDCOCK and LINTON, used for integrations by the Chebyshev approximation [20], series expansions [15] or adaptive quadrature algorithms [21]. The majority of external subroutines are from the book of Zhang & Jin [22], used for calculating some special functions, such as exponential integral function, error function, Gamma function, and many kinds of Bessel functions, based on continued fractions. Since so frequently called, the external subroutines of Bessel functions are hereby modified into several derivative versions, in order to improve the computation speed. Another external subroutine is from Mishonov & Penev [14], used for predicting the limit of a series in which the first several terms are known through the Epsilon Algorithm.

All the communications between subroutines in the present package are strictly restricted via explicit interfaces, without using any common data blocks. Therefore, it can be parallelized without any difficulty on Windows or Linux platform using parallelization techniques, such as OpenMP or MPI.

IV. Verifications of the Software Package

To verify the released package, a comparison is made with the Newman's method [12] using multi-dimensional polynomial approximations to calculate the Green's function and its derivatives in finite water depth. Comparison results are shown in Fig. 2, for a high pulsating frequency. Both the pulsating point source and the fluid field point are selected on the free surface in present tests, because the derivatives of free-surface Green's function are believed to be more difficult to evaluate when $z+\zeta=0$. As clearly shown in Fig. 2, even under such extreme conditions, perfect agreements can still be achieved between present results and those using Newman's method [12]. Periodic oscillations can be found in the derivatives of the free-surface Green's function. Worthwhile to note, the oscillation amplitude of the derivatives decreases with the increasing of *R*/*h*, indicating that the influence from a point source to a fluid field point decays with the horizontal distance.

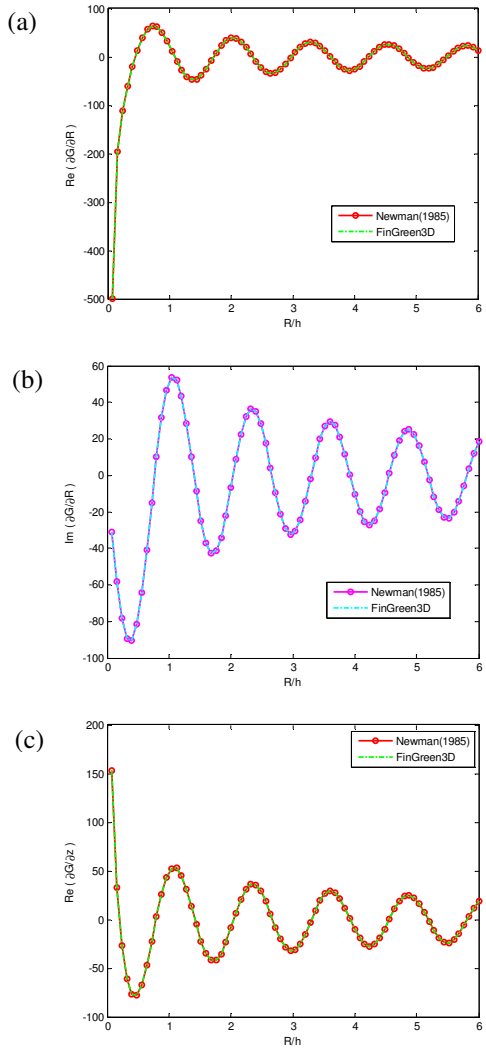

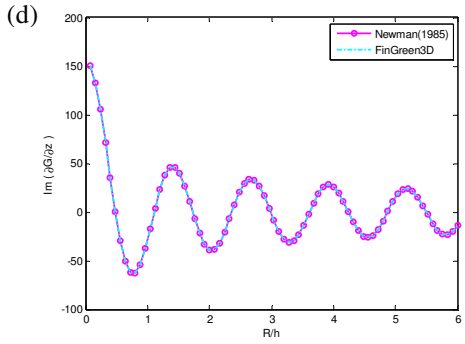

Fig. 2. Values of the gradient ∇G, as a function of *R/h*, when the point source and the field point locate at the free surface with a high pulsating frequency of $f = 1.1145\ \mathrm{s}^{-1}$ (i.e., wave number $v = 5.0\ \mathrm{m}^{-1}$): (a) real part of $\partial G/\partial R$; (b) imaginary part of $\partial G/\partial R$; (c) real part of $\partial G/\partial Z$; (d) imaginary part of $\partial G/\partial Z$.

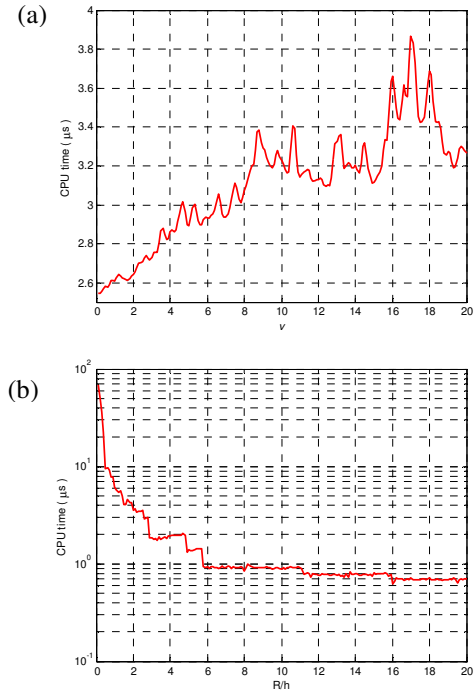

Fig. 3. Computation time for per implementation of FinGreen3D, as a function of wave number *v* (a) and normalised point distance *R/h* (b). The figures are obtained based on averaged CPU time of 1 million evaluations of FinGreen3D for each input wave number *v* and distance *R/h*, respectively.

Fig. 3 shows that, one implementation of the code, i.e., one evaluation of the Green's function and its derivatives consumes approximately 2~4 μs on a SONY laptop with an Intel(R) Core(TM) i7-2670QM CPU of 2.2 GHz and a 64-bit Windows 7 operating system. This low cost of computation means that for a practical offshore structure with nearly 5000 constant elements, 50~100s are sufficient for the computation of the influence matrix in each wave period on such a laptop. It will noteworthily facilitates the hydrodynamic analysis process for the practical offshore structures.

V. Applications to Waves-structure Interactions

The free-surface Green's function is the crucial fundamental component in the analysis of wave-structure interactions within potential-flow frame in the coastal/offshore renewable energies. Therefore, the present package FinGreen3D is successfully interfaced to a wave-structure-interaction panel code HAMS (Hydrodynamic Analysis of Marine Structures) [23].

A. *Case No.1: a submerged spherical wave energy converter*

A submerged sphere is presented as a benchmark test for validating the package. As a basic regular geometrical concept, the spherical shape is frequently employed to design wave energy converters (see e.g. [24], [25] and [26]). Parameters of the present benchmark case are listed as follows: associated with the sphere radius a, the ratio of radius to water depth is 0.3, and the ratio of immersion depth to radius is 1.5. Since the accuracy of the numerical results may reply on the mesh quality, firstly, a grid convergence test is conducted. Five mesh types are used, in which the number of panels increases as the grid divisions on the two directions (warp and weft) increase, see Table 2 for more details.

Table 2. Grid divisions on the sphere in the convergence test

Mesh	Warp Direction	Weft Direction	Number of Panels
Mesh 1	10	20	200
Mesh 2	20	30	600
Mesh 3	30	40	1200
Mesh 4	40	50	2000
Mesh 5	50	60	3000

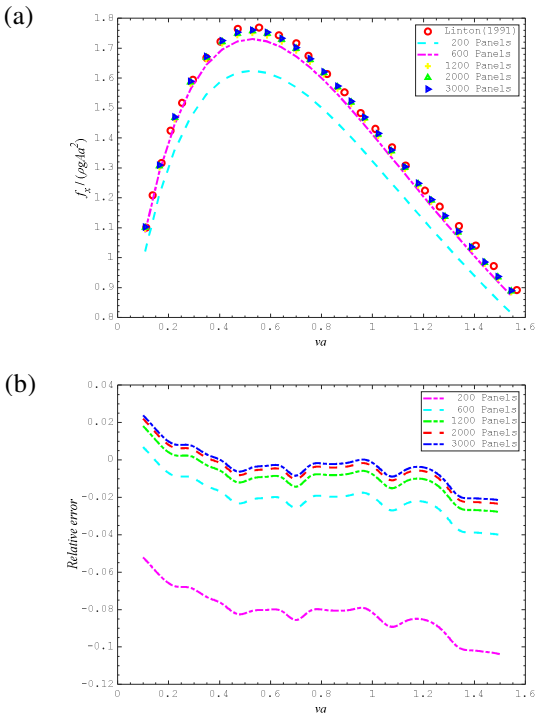

Fig. 4. Convergent test of the wave excitation force of a submerged sphere, as a function of the normalized radius *va*: (a) comparison between Linton's results [27] with respect to the number of panels, and (b) relative error analysis of (a).

Modulus of the horizontal exciting wave force of the submerged sphere is shown in Fig. 9(a). The comparison shows that the numerical result converges fast with respect to the number of panels. When the number of panels exceeds 600, the numerical result approaches almost very closely to the analytical solution [27]. This is further confirmed by the relative error analysis of the computation as shown in Fig. 9(b), the absolute relative error between the computation and the analytical solution is confined within 4% when the number of panels exceeds 600.

B. Case No.2: a semi-submersible offshore wind turbine with complex truss members

Computation of a complex-shaped platform with many truss members is conducted to show the capability of FinGreen3D in engineering applications. The platform was initially designed for supporting multiple diffuser-augmented wind turbines in Kyushu University [28, 29] at the 3rd development phase. It has three stacked large compound columns at the corners of the platform to support the turbine towers, three long pontoons which connect the columns and a large number of small bracings strengthening the platform structure. More details of the semisubmersible are listed in Table 3. The present floating wind turbine system was designed to operate in a water depth of 70 m.

Table 3. Definition of the full-scale properties of the semisubmersible

Properties	Values
Diameter of the Upper Columns	4.00 m
Diameter of the Lower Columns	11.5 m
Diameter of the Pontoons	1.70 m
Diameter of the Bracings	0.60 m
Number of the Trussed Bracings	66
Distance between Compound Columns	90.0 m
Draft in Operation	10.0 m
Platform Displacement	2.12×10^3 m^3

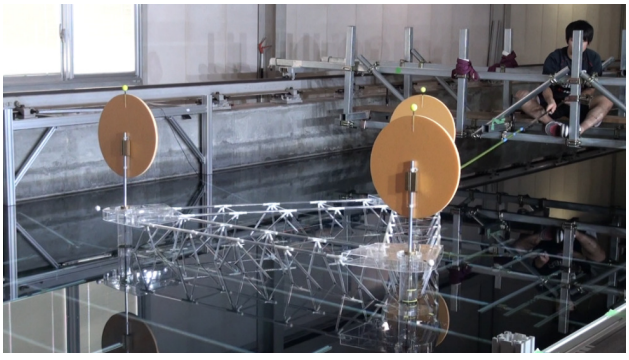

Fig. 5. Tank model test of the trussed semi-submersible floating wind turbine developed in Kyushu University, Japan.

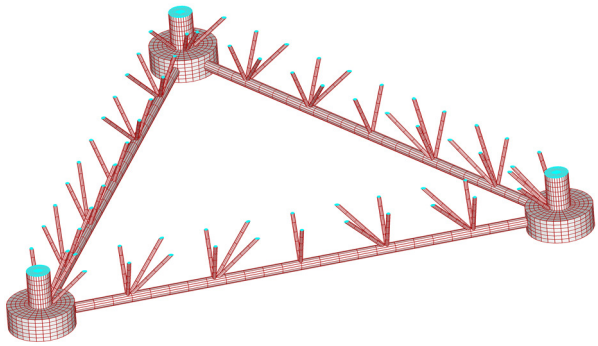

Fig. 6. Mesh of the submerged part of the platform in altogether 5040 panels, with 4110 panels on the immersed body surface (in dark red color) and 930 panels on the water planes (in light blue color).

A 1/50-scale model experiment has been conducted at the towing tank of Research Institute for Applied Mechanics (RIAM), Kyushu University, as displayed in Fig. 5. Added mass and radiation damping coefficients in heave motions are measured by the forced excitation test. Wave exciting forces are measured by fixing the model in the regular waves. Numerical computations are performed by incorporating and compiling the FinGreen3D & HAMS codes. A mesh grid convergent test is performed in association with a validation by the experiment measurement. The meshes are divided into four types as shown in Table 4, varying on the grid resolution of different members, from coarse meshes to fine meshes. A representative of the fine meshes is displayed in Fig. 6. Comparison between the numerical results and the model test data are given in Fig. 7, where the quantities are normalized by the water density ρ, the gravity acceleration g and the platform displaced volume V. The comparison shows that accuracy of the numerical results depends heavily on the grid resolution, especially in the gravity direction in the diffraction problem (or the heave mode in the radiation problem). As the grids become finer, the numerical results get closer to the experiment data. Generally, the agreement between the two results is satisfactory.

Table 4. Grid divisions on members of the platform in the test case

Mesh	Main Columns			Pontoons			Bracings		
	S	R	T	S	R	T	S	R	T
Mesh 1	8	4	4	8	4	6	5	2	4
Mesh 2	12	4	4	8	4	10	8	2	5
Mesh 3	24	4	4	12	4	10	10	2	5
Mesh 4	30	6	6	15	4	12	10	2	5

Note: In Table 4, the abbreviations “S”, “R” and “T” stand for divisions along the directions of “circumferential”, “radial” and “draft”, respectively.

(a)

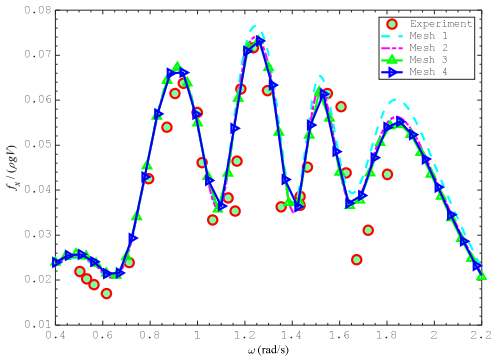

(b)

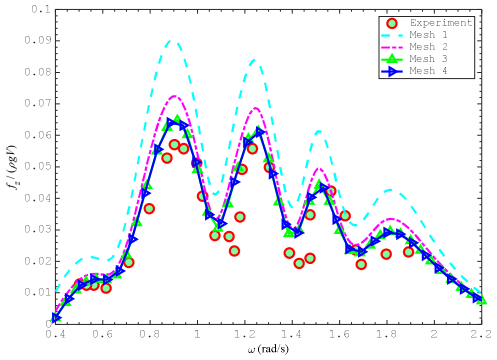

Fig. 7. Wave forces upon the triangular platform as a function of the wave angular frequency ω: (a) excitation force in x-direction, (b) excitation force in z-direction. "Mesh 1", "Mesh 2", "Mesh 3" and "Mesh 4" denote numerical results computed by the FinGreen3D & HAMS codes, using meshes specified in Table 4. Solid dot denotes experiment data measured from the tank model test.

Fig. 8 shows contour plots of the scattered free surface elevation (normalized by the incident wave amplitude) in the vicinity of the platform. As shown in Figs. 8(a), when the waves incident at a lower wave frequency, the scattered wave fields are relatively flat. In other words, the free surface has not been changed noticeably by the scattered waves. That is because waves of a large wavelength can easily transmit over a floating 'obstacle' of a smaller dimension. The elevations at a relative higher wave frequency are shown in Figs. 8(b), where the wavelength is more comparable to the physical dimension of the platform.

(a)

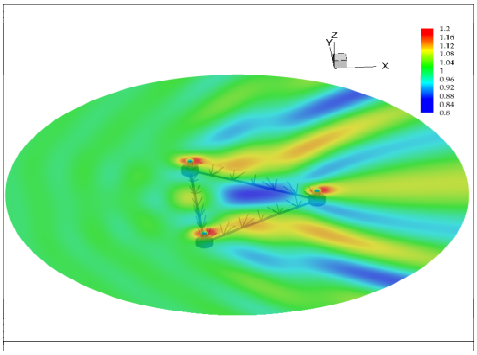

(b)

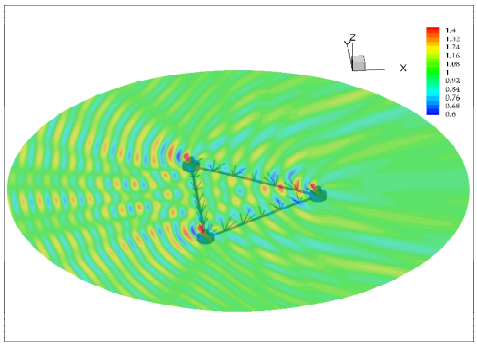

Fig. 8. Contour plot of free surface elevation (normalized by the incident wave amplitude) in the conditions of: (a) ω=0.1, and (b) ω=0.3.

In Fig. 18(a) and (b), the wave field is symmetric because of symmetry of the platform with respect to the wave incident direction. In addition, it can be noticed that the largest enhancement of the elevation always occurs at the neighbourhood of the three large compound columns, regardless of the wave frequency, showing that the diameter of column is the main factor of scattering. As the waves go far away from the structure, the amplitude of elevation decreases substantially, which agrees with our knowledge in common practice.

C. *Case No.3: a next-generation floating wind turbine moored by single-point turret system*

A new-type SCD®-Nezzy offshore floating wind turbine which is currently under demonstration in Hiroshima of Japan is used as another application case, as shown in Fig. 9. The two-bladed floating wind turbine has the ability of self-aligning with the change of wind direction, attributed to the latest technologies of an airfoil-shaped leaning tower and a single-point turret system. Its Y-shaped floating foundation consists of three separate leaning columns, three horizontal pontoons, and a center column being also the lower part of the tower. The spreading mooring lines are allocated to a single fairlead at the end of the Y-shaped foundation which has a torsional degree of freedom. The floating wind turbine is designed to operate in a water depth of 52 m, at the coastal area of Japan.

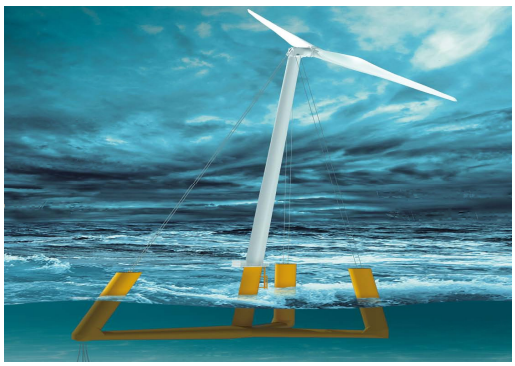

Fig. 9. Schematic of the 3.0 MW SCD®-Nezzy floating wind turbine [30]

The floating foundation is discretized by a pretty fine mesh, with the consideration of the wave orbital trajectory and the local details, as displayed in Fig. 10. Since the circular orbits of the water particles decrease with the increase of the immersion depth in water, and decrease to zero if the immersion depth

exceeds half wave length, the mesh grid density is specifically generated to be the largest in the region close to the mean sea level and decreasing with the depth. In addition, since at the turret mooring point the structure geometry has a complex local detail, the mesh grid there is intentionally generated to be denser than its neighboring areas.

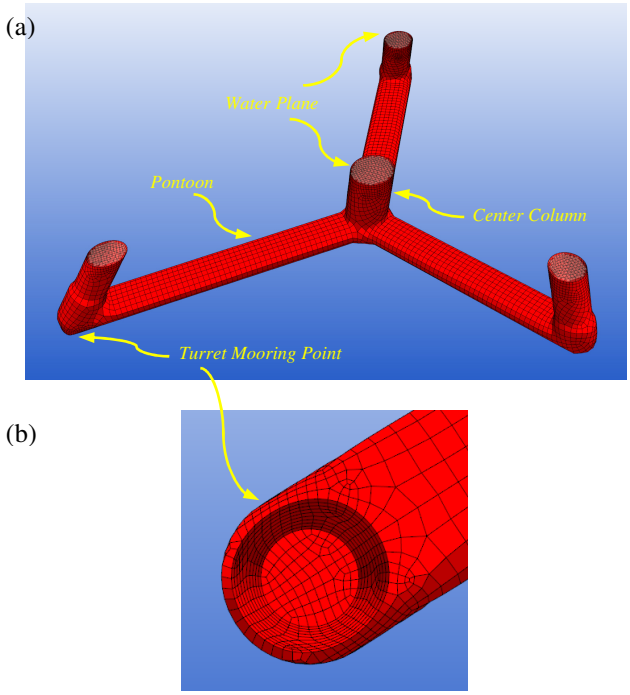

Fig. 10. Mesh of the SCD®-Nezzy floater: (a) perspective view of the entire floater and (b) local bottom view of the turret mooring point

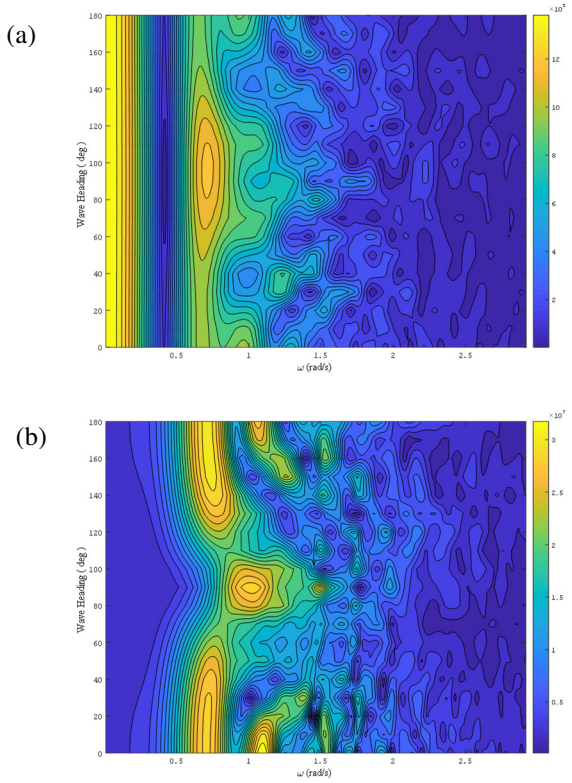

Fig. 11. Modulus of the wave excitation force/moment acting on the SCD®-Nezzy floater as a function of the wave angular frequency ω: (a) heave wave excitation force, and (b) pitch wave excitation moment.

Fig. 10 shows the distribution of wave excitation force/moment on the SCD®-Nezzy floater with respect to the wave angular frequency and wave headings. It is seen that due to the symmetry of the SCD®-Nezzy floater, the distributions are symmetric with respect to the line of wave heading $\beta = 90^{\circ}$. Note that there are several major regions where the floater is attacked heavily by the wave force/moment. For the surge wave force, the maximum value occurs at the places of $0^{\circ} < \beta < 40^{\circ}$, $140^{\circ} < \beta < 180^{\circ}$ and $0.8 < \omega < 1.6$. For the heave wave force, the maximum value occurs at two major places, i.e., the small band $0 < \omega < 0.2$ and the region in the neighborhood of the peak at $\beta = 90^{\circ}$ and $\omega = 0.65$. For the pitch wave moment, the maximum value occurs in the frequency band $0.5 < \omega < 1.5$, and near the wave heading $\beta = 90^{\circ}$ as well as the regions of $0^{\circ} < \beta < 40^{\circ}$, $140^{\circ} < \beta < 180^{\circ}$. Outputting such distributions of wave excitation force/moment has significant meanings to the design of such floaters in practice.

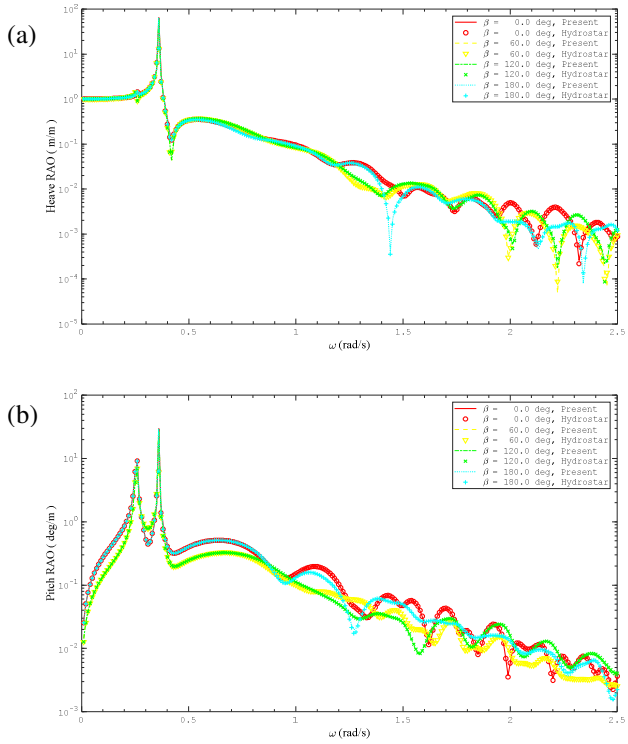

Fig. 12. Motion response of SCD®-Nezzy floating wind turbine, as a function of the wave angular frequency ω: (a) heave response; and (c) pitch response. The results denoted by symbols are computed by the commercial version of the Hydrostar® software.

Fig. 12 shows the analysis of response amplitude operators (RAOs) on the motions of the SCD®-Nezzy floating wind turbine, and a comparison between the present results and those computed by the commercial software Hydrostar®. The motion RAOs are measured by the motion response amplitude over the incident wave amplitude. In order to show clearly the differences, the data are plotted using the semi-logarithmic coordinate. It is seen that, except for some small differences

which are hard to distinguish, the two results coincide perfectly well with each other. The peaks at the resonance region ($0.0<\omega<0.5$) predicted by the two software are also in quite good agreements. The motion RAOs generally decrease with the increase of the wave angular frequency, to a negligible level when the wave angular frequency exceeds 2.0. This is also in consistence with the energy distribution in the ocean spectrums, e.g., Jonswap spectrum, Pierson–Moskowitz spectrum, etc., which almost concentrates within the angular frequency band of [0, 2.0].

VI. Conclusions

A reliable numerical software package - FinGreen3D has been presented, using a region-decomposition strategy for evaluation of the free-surface Green's function in moderate depth, which is widely considered as the essential part but is difficult to be calculated in the analysis of wave-structure interactions. The advantage of the present method is the high accuracy of computation, and also that it is relatively much cheaper than the computational fluid dynamics (CFD) methods due to its fast evaluation speed. The present method is appropriate for large-scale floating structures on the purpose of quickly evaluating their integral performance with respect to a batch of input environmental conditions/parameters. The package is written using Fortran 90 with optimized structure and can be implemented in either Windows or Linux. The package structure and its interface have been clearly illustrated so as to make it well understandable by the readers/users. The accuracy and efficiency of the present software package have been confirmed by extensive validations. The software package code can be distributed freely for either academic research or industrial application purpose.

Acknowledgment

This research is supported in part by Grants-in Aid for Scientific Research (B), MEXT (no. 15H04215). We would also like to thank the NEDO (New Energy and Industrial Technology Development Organization) of Japan in providing an industrial application for validation of this software package. The first author also gratefully acknowledges the International Conference Travel Expenses Support provided by the Kyushu University Research Activity Support Program.

References

[1] Kammen DM, Sunter DA. City-integrated renewable energy for urban sustainability. Science 2016; 352: 922-928.

[2] Colmenar-Santos A, Perera-Perez J, Borge-Diez D. Offshore wind energy: A review of the current status, challenges and future development. Renewable and Sustainable Energy Reviews 2016; 64: 1-18.

[3] Lehmann M, Karimpour F, Goudey CA, Jacobson PT, Alam MR. Ocean wave energy in the United States: Current status and future perspectives. Renewable and Sustainable Energy Reviews 2017; 74: 1300-1313.

[4] Khan N, Kalair A, Abas N, Haider A. Review of ocean tidal, wave and thermal energy technologies. Renewable and Sustainable Energy Reviews 2017; 72: 590-604.

[5] Benitz MA, Lackner MA, Schmidt DP. Hydrodynamics of offshore structures with specific focus on wind energy applications. Renewable and Sustainable Energy Reviews 2015; 44: 692-716.

[6] Wang X, Zeng X, Li J, Yang X, Wang H. A review on recent advancements of substructures for offshore wind turbines. Energy Conversion and Management 2018; 158: 103-119.

[7] Liu Y, Li S, Yi Q, Chen D. Developments in semi-submersible floating foundations supporting wind turbines: A comprehensive review. Renewable and Sustainable Energy Reviews 2016; 60: 433-449.

[8] Oh KY, Nam W, Ryu MS, Kim JY, Epureanu BI. A review of foundations of offshore wind energy convertors: Current status and future perspectives. Renewable and Sustainable Energy Reviews 2018; 88:16-36.

[9] Astariz S, and Iglesias G. Selecting optimum locations for co-located wave and wind energy farms. Part I: The Co-Location Feasibility index. Energy Conversion and Management 2016; 122: 589-598.

[10] Astariz S, and Iglesias G. Selecting optimum locations for co-located wave and wind energy farms. Part II: A case study. Energy Conversion and Management 2016; 122: 599-608.

[11] Li L, Gao Y, Yuan Z, Day S, Hu Z. Dynamic response and power production of a floating integrated wind, wave and tidal energy system. Renewable Energy 2018; 116: 412-422.

[12] Newman JN. Algorithms for free-surface Green function. Journal of Engineering Mathematics 1985; 19: 57-67.

[13] Wynn P. On a Device for Computing the em(Sn) Transformation. *Mathematics of Computation* 1956; 10(54): 91-96.

[14] Mishonov T, Penev E. Thermodynamics of Gaussian fluctuations and paraconductivity in layered superconductors. *Int. J. Mod. Phys. B* 2000; 14: 3831-3879.

[15] Pidcock MK. The calculation of Green functions in three dimensional hydrodynamic gravity wave problems. *International Journal for Numerical Methods in Fluids* 1985; 5: 891-909.

[16] Linton CM. Rapidly convergent representations for Green functions for Laplace's equation. *Proceedings of The Royal Society A: Mathematical, Physical and Engineering Sciences* 1999; 455: 1767-1797.

[17] Ewald P. Die berechnung optischer und electrostatischer gitterpotentiale. *Annalen der Physik* 1921; 369: 253-287.

[18] Newman JN. Distributions of sources and normal dipoles over a quadrilateral panel. *Journal of Engineering Mathematics* 1986; 20: 113-126.

[19] Sun L, Teng B, Liu CF. Removing irregular frequencies by a partial discontinuous higher order boundary element method. *Ocean Engineering* 2008; 35: 920-930.

[20] Newman JN. The approximation of free-surface Green functions. Retirement Meeting for Professor Fritz Ursell, University of Manchester, published in "*Wave Asymptotics*" edited by Martin PA and Wickham GR, pp. 107-135. Cambridge University Press, Cambridge; 1992.

[21] Liu Y, Gou Y, Teng B, Yoshida S. An Extremely Efficient Boundary Element Method for Wave Interaction with Long Cylindrical Structures Based on Free-Surface Green's Function. *Computation* 2016; 4(3): 36.

[22] Zhang S, Jin JM. Computation of special functions. Wiley-Interscience; 1996.

[23] Liu Y, Hu C, Sueyoshi M, Iwashita H, Kashiwagi M. Motion response prediction by hybrid panel-stick models for a semi-submersible with bracings. Journal of Marine Science and Technology 2016; 21(4): 742-757.

[24] Vicente PC, Falcão AF, Justino PA. Nonlinear dynamics of a tightly moored point-absorber wave energy converter. Ocean engineering 2013; 59: 20-36.

[25] Sergiienko NY, Cazzolato BS, Ding B, Hardy P, Arjomandi M. Performance comparison of the floating and fully submerged quasi-point absorber wave energy converters. Renewable Energy 2017; 108: 425-437.

[26] Bharath A, Nader JR, Penesis I, Macfarlane G. Nonlinear hydrodynamic effects on a generic spherical wave energy converter. Renewable Energy 2018; 118: 56-70.

[27] Linton CM. Radiation and diffraction of water waves by a submerged sphere in finite depth. *Ocean Engineering* 1991; 18: 61-74.

[28] Bremen M. Japan's Floating Offshore Wind Projects: An Overview; 2013.

[29] Hu C, Sueyoshi M, Liu C, Liu Y. Hydrodynamic analysis of a semi-submersible type floating wind turbine. In: Proc. of the Eleventh ISOPE Pacific/Asia Offshore Mechanics Symposium, Shanghai, China; 2014.

[30] Website (http://www.scd-technology.com/scd-technology-scd-nezzy/)